Bias Prediction for MEMS Gyroscopes

Martti Kirkko-Jaakkola, Jussi Collin, and Jarmo Takala, *Senior Member, IEEE*

***Abstract*—MEMS gyroscopes are gaining popularity because of their low manufacturing costs in large quantities. For navigation system engineering, this presents a challenge because of strong nonstationary noise processes, such as $1/f$ noise, in the output of MEMS gyros. In practice, on-the-fly calibration is often required before the gyroscope data are useful and comparable to more expensive optical gyroscopes. In this paper, we focus on an important part of MEMS gyro processing, i.e., predicting the future bias given a calibration data with known (usually zero) input. We derive prediction algorithms based on Kalman filtering and the computation of moving averages, and compare their performance against simple averaging of the calibration data based on both simulations and real measured data. The results show that it is necessary to model fractional noise in order to consistently predict the bias of a modern MEMS gyro, but the complexity of the Kalman filter approach makes other methods, such as the moving averages, appealing.**

***Index Terms*—$1/f$ noise, calibration, gyroscopes, microelectromechanical systems, navigation, stochastic processes.**

I. Introduction

ALTHOUGH today's MEMS gyroscopes are inferior to optical sensors from the accuracy point of view, their low cost, tiny size, low power consumption, and suitability to production in large quantities are undeniable advantages that have enabled their integration into a variety of low-cost consumer devices [1]–[3]. It is clear that the traditional inertial navigation mechanization [4] is not directly suitable for MEMS-based inertial units, but by adding on-the-fly calibration [5], nonholonomic constraints [6], and, preferably, sensors measuring the traveled distance directly, the accuracy of the navigation solution approaches a level that is suitable for many applications. Recently introduced temperature-conditioned MEMS gyros [7] avoid the most significant external error source, i.e., the effect of the ambient temperature in the gyro bias [8]. Studying the noise processes of temperature-controlled MEMS sensors is of great interest because the external factors are negligible and the remaining processes can be considered purely stochastic.

The quality of a MEMS gyro is often defined by the magnitude of the constant additive bias. In positioning and navigation applications, the angular rate measurement output by the gyro is integrated to obtain an angle measurement; any constant bias error in the angular rate is then integrated into a linearly increasing angle error. The bias can be eliminated by means of carouseling [9] or direct estimation. In strapdown applications, carouseling is not an option because of the high power consumption, large size, and extra weight of the gimbal assembly required for slewing the sensor.

If the gyro error consisted of a constant bias and additive white noise only, the bias could be calibrated out by recording a long sequence of data with known input. However, this does not work in practice because the bias of a MEMS gyro has a significant day-to-day component that changes every time the device is powered up. Another reason is that the MEMS gyro error processes are clearly nonstationary and, therefore, cannot be separated into a constant part and a white noise part. Thus, the calibration should be done whenever possible, i.e., whenever the input rotation rate is known. For land vehicle navigation, a practical scenario is to calibrate the gyro bias whenever the vehicle is at standstill; stationarity can be detected based on, e.g., an odometer. In this paper we will focus on this scenario, the bias calibration problem then being a prediction problem given the gyro data of the standstill period.

Bias instability can be defined as "the random variation in bias as computed over specified finite sample time and averaging time intervals. This nonstationary (evolutionary) process is characterized by a $1/f$ power spectral density" [10]. A large amount of literature is devoted to understanding $1/f$ (flicker) noise and other fractional noise processes [11]–[14]. As shown by Voss [15], the Allan variance of $1/f$ noise is constant; without temperature control, external temperature effects mask this behavior, as can be seen in Fig. 1. The Allan variance of the MEMS gyro without temperature control shows an increasing trend at long averaging times. Because of the low availability of temperature-conditioned sensors, MEMS navigation research has been concentrating on other types of errors.

The contribution of this article is to link the properties of $1/f$ noise and the prediction problem involved in gyro bias calibration. We first derive the optimal Kalman predictor for the $1/f$ noise model. Then, noting the computational complexity of the Kalman predictor, we derive a simpler predictor based on moving averages and compare the performance of these prediction algorithms. According to the experimental results, taking the $1/f$ characteristic of bias instability into account enables more accurate predictions of the gyro bias, thus improving the accuracy of the navigation system for which the gyro is being used.

II. Related Work

Calibration methods for gyroscopes have been extensively researched in the literature. For example, when integrating a traditional inertial navigation mechanization with satellite positioning, the inertial sensor errors can be estimated on

Manuscript received November 1, 2011; revised December 16, 2011; accepted January 16, 2012. This work has been partially funded by the NPI programme of the European Space Agency and by the Finnish Funding Agency for Technology and Innovation under research funding decision 40043/10.

The authors are with the Department of Computer Systems, Tampere University of Technology, P.O. Box 553, FI-33101 Tampere, Finland (e-mail: martti.kirkko-jaakkola@tut.fi; jussi.collin@tut.fi; jarmo.takala@tut.fi).

the fly using a Kalman filter [16]. In the context of MEMS gyros, day-to-day errors are often so significant that an initial calibration is necessary. In principle, estimating the gyro bias is straightforward given the true angular rate. A common approach is to average a sequence of data measured while the sensor is standing still [17]–[19]; this way, the input is constant (equal to the component of Earth rotation parallel to the sensing axis) and the obtained average is used as a prediction of the future bias. While modeling the bias this way, i.e., as piecewise constant, can be optimal for stationary errors, the nonstationarity of the $1/f$ component of the gyro signal causes problems with this approach.

Another approach to model the bias instability process is to use an autoregressive (AR) model. For instance, [20] investigates fitting AR models of order up to four on data where wavelet denoising has been applied. A least-squares AR model fitting procedure is described in [21] where using a fourth-order AR model is proposed. In [22], an AR model of order 120 was constructed using system identification methods.

In the articles described above, however, the AR model was not tuned for $1/f$ noise only, but also for the effect of temperature changes and other factors that tend to dominate the $1/f$ phenomenon at long averaging times. In contrast, in this paper, the model is built based on the properties of $1/f$ noise instead of fitting coefficients on measured data, and we use a temperature-conditioned gyro to minimize the effect of long-term errors that would otherwise mask the $1/f$ behavior.

III. Gyroscope Noise Processes

The output of a gyro is an angular rate measurement which can be modeled at time t as [23]

$$y(t) = \mathrm{M}\boldsymbol{\omega}(t) + \epsilon(t) \tag{1}$$

where M is the 1×3 cross-coupling and scale factor error matrix, $\boldsymbol{\omega}(t)$ is the angular rate vector between the sensor body and an inertial reference frame, and $\epsilon(t)$ is the additive measurement error. In this article, we neglect the cross-coupling and scale factor effects and divide the additive error $\epsilon(t)$ into three components: constant bias, uncorrelated (white) noise, and $1/f$ noise. The influence of the most significant error sources can be characterized by computing the Allan variance of the sensor signal, which is discussed below. It should be noted that Allan variance is not the only available method for identifying gyro error structures [24]; nevertheless, it is recommended in [25].

A. Allan Variance

Also known as the two-sample variance, the Allan variance was originally developed for describing the stability of frequency standards [26]. The Allan variance σ_A^2 is a function of the averaging time τ, computed as

$$\sigma_A^2(\tau) = \frac{1}{2\,(N-1)} \sum_{i=1}^{N-1} \left(\bar{y}(\tau)_{i+1} - \bar{y}(\tau)_i\right)^2 \tag{2}$$

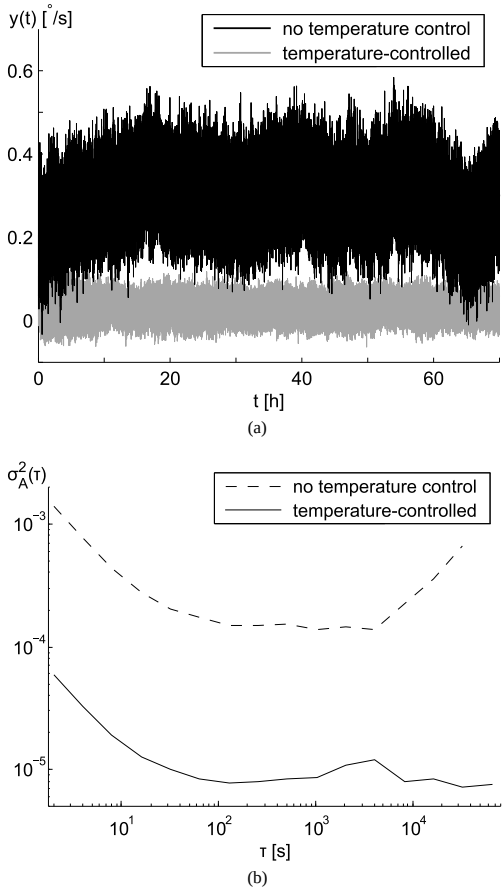

Fig. 1. Effect of temperature control on Allan variance. (a): Angular rate as measured by two gyroscopes; (b): the corresponding Allan variances.

where the values of $\bar{y}(\tau)_i$ are obtained by dividing the data y into N disjoint bins of length τ; $\bar{y}(\tau)_i$ is the average value of the ith bin.

Allan variance is usually visualized as a log-log graph. Given the Allan variance plot of a sensor, it is easy to find the optimal averaging time that minimizes the effect of uncorrelated and time-correlated errors: at short averaging times, uncorrelated noise dominates the output, whereas long averaging times are prone to drifting errors. Fig. 1 shows two sets of data and the corresponding Allan variance curves; it can be seen that for both data sets, an averaging time of 1000 seconds would be a reasonable choice.

B. Gyroscope Noise Components

The accuracy of MEMS gyroscopes is degraded by many error sources and the most significant is bias. A comprehensive description of the different error sources is given in [25, Annex C] in the context of laser gyros but the same error sources apply to MEMS gyros as well. Long-term bias can

be calibrated fairly accurately but there is always a day-to-day bias component. When the actual input, i.e., the angular rate, is zero, the bias can be estimated by averaging the sensor output. However, averaging cannot work perfectly because of certain fluctuating (not necessarily zero-mean) errors in the signal.

White noise (also referred to as angle random walk [25]), originating from, e.g., thermal noise [27], is a simple stochastic process that consists of independent and identically distributed samples. Its variance is inversely proportional to the averaging time, thus the effect of white noise can be seen as an initial negative slope in the Allan variance graph.

$1/f$ *noise*, however, is a more complicated stochastic process. Although discovered almost a century ago [11], [28] and encountered in many different contexts, such as semiconductors, river Nile's flood levels, and pitch fluctuations in music, its origin is not exactly known [15]. As opposed to uncorrelated white noise, $1/f$ noise is a long-memory process, i.e., the mutual correlations between samples decay slowly [29]. It can be modeled as an ARFIMA$(0, d, 0)$ process (*autoregressive fractionally integrated moving average*) whose dth difference is a white noise process. The dth difference of the sequence $x_0, x_1, \ldots$ is computed as [14], [29], [30]

$$\Delta^d x_k = \sum_{i=0}^{k} \left((-1)^{k-i} \frac{\Gamma(k-i+d)}{\Gamma(k-i+1)\Gamma(d)} x_i \right) \tag{3}$$

where $\Gamma(\cdot)$ denotes the gamma function. Another quantity to characterize a long-memory process is the Hurst exponent H, which is related to the order d by [14]

$$d = H - \frac{1}{2}. \tag{4}$$

The Hurst exponent is commonly encountered in literature where long-memory processes are discussed but, in this article, d will be used as the memory parameter.

Another error source in the sensor output is *rate random walk* (RRW), which is caused when the bias changes (slowly) with time. This can be due to, e.g., aging of the sensor components or changes in the temperature of the gyro; MEMS sensors are typically highly sensitive to temperature variations [8]. RRW causes a positive slope to the Allan variance at long averaging times. Unlike $1/f$ noise, RRW is a Markov process, i.e., memoryless: its value at step $k+1$ only depends on the value at step k, not on any other (past or future) values.

Since white noise causes imprecision at short averaging times and RRW degrades the accuracy at long averaging times, the optimal averaging time is found between these two. The minimum of the Allan variance of a gyro is called the *bias instability* and can be used as a measure of the power of $1/f$ noise [25].

IV. Proposed Gyroscope Error Predictors

In this section, we present two approaches of predicting the evolution of the bias: one based on Kalman filtering and one based on computing a moving average. In Section V, these predictors will be compared to the simple approach of averaging the entire calibration data.

A. Kalman Filter Approach

The Kalman filter (KF) [31] is a tool for analyzing dynamic systems and is widely used in positioning and navigation, along with its nonlinear extensions. Given the observation and system evolution models and an initial state, it estimates the state of the system. In this study, the KF is employed for tracking $1/f$ noise.

As state variables we take the current and previous noise realizations. This means that the length of the state vector increases at each time step; the solution cannot be optimal unless the state vector is infinite-dimensional [32]. It has been shown that one state variable per decade of samples (i.e., one for the most recent sample, one for the latest 10 samples, one for the last 100 etc.) are sufficient to characterize a $1/f$ process [13], [33]. Nevertheless, in this study, one state variable was used for each sample. Therefore, the state is propagated from sample $(j-1)$ to j as a fractional integral

$$\mathbf{x}_j = \begin{bmatrix} \mathrm{I} \\ \mathbf{f}_j^T \end{bmatrix} \mathbf{x}_{j-1} \tag{5}$$

where I is the identity matrix, ^{T} denotes the transpose, and the ith element of the vector $\mathbf{f}_j \in \mathbb{R}^{j-1}$ is obtained as [14], [29]

$$[\mathbf{f}_j]_i = -\frac{\Gamma(j-i-d)}{\Gamma(j-i+1)\Gamma(-d)}. \tag{6}$$

The formula is remarkably similar to (3)—only the sign of d is different. This formula is, in principle, only valid for $-1/2 < d < 1/2$, i.e., when the process is stationary and invertible; for $d \geq 1/2$, these conditions do not hold [14]. Therefore, the prediction obtained using the values (6) may be biased if $d = 1/2$ is used. For covariance propagation, the variance of the driving noise of the $1/f$ noise needs to be known.

The coefficients obtained from (6) have absolute value less than one. Thus, as time passes, the forecast eventually decays towards zero. Nevertheless, it would be desirable that the prediction would tend towards the sample mean instead. This can be changed by taking the sample mean as an additional state variable and modeling the bias as the sum of $1/f$ noise and the sample mean. This makes observation updates straightforward as well, as long as the variance of white noise is known. If it is not given in the specifications of the gyro, it can be estimated from the Allan variance.

B. Moving Average Approach

As the optimal prediction using Kalman filter is too complex for practical implementation, we introduce simpler predictor based on moving averages. Assuming that the Allan variance of the noise process is constant, i.e.,

$$\frac{1}{2\,(N-1)} \sum_{i=1}^{N-1} \left(\bar{y}(\tau)_{i+1} - \bar{y}(\tau)_i \right)^2 = \beta \quad \forall \tau, \tag{7}$$

and further assuming that the increments in the block averages $\bar{y}_i$ are mutually independent, the best predictor for $\bar{y}(\tau)_{i+1}$ given $\bar{y}(\tau)_i$ would be $\bar{y}(\tau)_i$ itself. Thus the

prediction of τ future samples would be the mean of past τ samples. Generalizing this leads to the simple predictor

$$\hat{y}_j = \frac{1}{j} \sum_{i=-j+1}^{0} y_i \tag{8}$$

where $j = 0$ is the time index of the last calibration sample. This is by no means an optimal predictor for $1/f$ noise, as the second assumption (independence of the increments) does not hold. However, the predictor is very easy to implement and the results presented in Section V show that its prediction performance is not far from the Kalman predictor values. If the calibration period is shorter than the navigation mission (as often is the case), the simple average of the calibration data

$$\hat{y}_j = \frac{1}{k} \sum_{i=-k+1}^{0} y_i, \quad j \geq k, \tag{9}$$

where k is the length of calibration data, can be used to extend the moving average.

V. Experiments

The performance of the proposed predictors was evaluated by running them on a large number of data sets with zero angular rate input; there were both artificial data sets and authentic gyroscope data. In each run, the first half of the data were used for calibration, based on which the evolution of the bias was predicted in the latter half. This resembles the scenario of driving a vehicle: occasionally, the vehicle must stop, e.g., at crossroads, which gives an opportunity for a zero-velocity update. Another application is pedestrian walking [34] where there is a stance phase followed by a swing phase, although the durations of the phases considerably shorter.

The artificial data were generated as ARFIMA(0, 1/2, 0) sequences according to (3) and the authentic data originated from an immobile gyro; the data sets used in Section V-B contained $2\,400$ samples each, whereas the results of Section V-C are based on $2\,000$-sample-long sets. The angular rate caused by the rotation of Earth was not treated in any way—since the gyro was static during the experiments, the effect of Earth rotation was constant and can be seen as a part of the bias. In all test runs, an integration order $d = 1/2$ was used for modeling $1/f$ noise; this is not necessarily optimal for the real data as some other choice of d could model the gyro noise correlations better. However, the exact local Whittle estimate [12] of the gyro data used is 0.535, which suggests that the chosen value of d is reasonable.

In theory, because of the zero angular rate, the integral (in discrete time, the sum) of the difference between the data and the predicted bias should equal zero. Therefore, we use two error metrics to quantify the prediction error:

- integrated error (IE): the sum of the prediction errors, i.e., the difference between the data and the predicted bias
- root sum of squared errors (RSSE): the sum of the squares of the prediction errors.

Obviously, the IE describes the accumulated angle error after the prediction phase, and the absolute value of the IE is what we ultimately want to minimize. The RSSE is computed for validation purposes: the KF should, in theory, minimize the error variance among linear estimators. Therefore, if the KF does not yield the lowest RSSE, the models used in the KF are probably incorrect.

In the following sections, we first discuss the choice of the gyroscope. Then, we study the behavior of the proposed predictors in example runs based on both artificial and authentic data. Finally, the performance of the predictors are compared in an extensive batch test in order to assess how the methods perform in general.

A. Choosing the Sensor

In order to get gyroscope data whose power spectral density obeys a $1/f$ shape as well as possible (when properly averaged), we need a gyroscope with negligible RRW. As shown in Fig. 1, this can be achieved even using a MEMS sensor if it is temperature-conditioned: in the Allan variance curve of the temperature-controlled gyro, no RRW slope is visible at averaging times smaller than 10^5 seconds and the Allan variance is almost constant for averaging times longer than 10^2 seconds. The same figure shows that this is certainly not the case for the gyroscope that is not temperature-conditioned: its Allan variance starts to increase at averaging times longer than approx. $4{\cdot}10^3$ seconds because of RRW. The temperature-conditioned gyro appearing in Fig. 1 is [7] and the other gyro is [35].

In applications, temperature-conditioning has its drawbacks; for instance, the power consumption and physical size of the oven where the sensor is located may prevent using the technology in mobile devices. However, these considerations are beyond the scope of this paper.

B. Example Runs

Fig. 2 shows the results of applying the estimation methods discussed in Section IV on artificial data. The samples were generated by half-integrating Gaussian white noise according to (3) and adding a constant bias; no other components, such as additive white noise or random walk, were introduced. It can be seen that the KF estimate (Fig. 2a) decays smoothly towards the mean of the calibration data while the moving average (Fig. 2b) is more oscillatory, especially at the beginning where the average is computed over a smaller number of samples.

With this data set, the KF performs better in terms of both IE and RSSE: the KF error integrates to -201 (dimensionless; no units assumed for the simulated data) while the integrated moving average error is 535. The RSSE values are 123 and 127, respectively. For comparison, the errors obtained by using the mean of the calibration data as the sole estimate of the bias were -2910 (integrated) and 146 (RSSE). Hence, the improvement is obvious in this case. Fig. 2a also shows the two-sigma confidence interval of the KF estimate; the bounds seem to agree with the data.

An example of estimator performance using real gyro data is shown in Fig. 3. To be able to use the KF, the standard deviations of additive white noise and the driving noise of the $1/f$ process had to be estimated first. The values $45°$/h and $14°$/h, respectively, were found to be appropriate, which

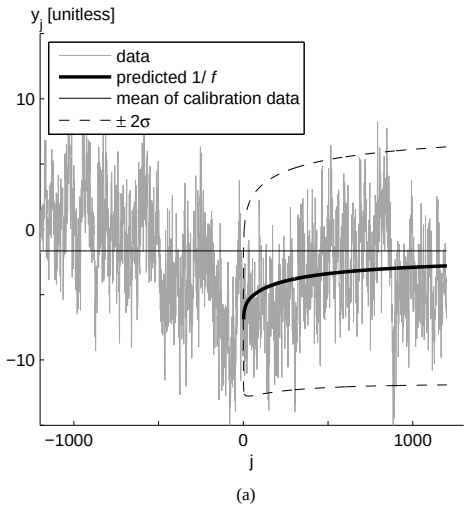

(a)

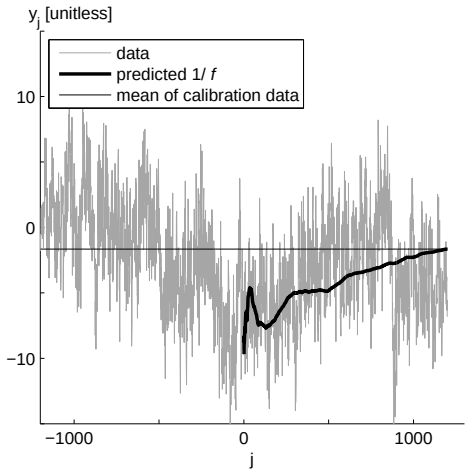

(b)

Fig. 2. Prediction results for simulated data (no white noise): (a) Kalman filter; (b) moving average.

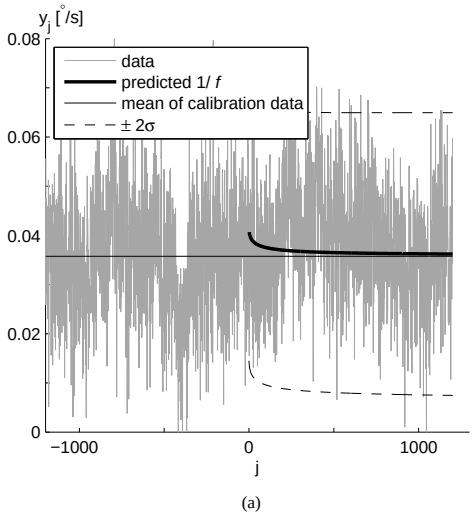

(a)

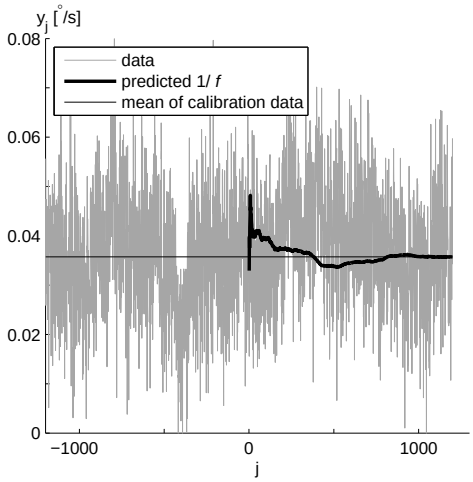

(b)

Fig. 3. Prediction results with authentic data: (a) Kalman filter; (b) moving average.

is reflected by the consistency of the two-sigma confidence interval estimate in Fig. 3a. It should be noted that these are the confidence bounds of the signal including white noise; the confidence interval for the $1/f$ component only would be narrower.

The KF outperforms the moving average and calibration data mean with this set of data, too. The IE and RSSE for the KF estimate are $2.46°$ and $0.410°$, respectively. The corresponding values for the moving average estimate are $3.13°$ and $0.424°$, and for the mean of the calibration data, $3.55°$ and $0.415°$. In this test case, the mean of the calibration data was a better estimator in the RSSE sense than the moving average.

C. Batch Test

In the example cases described above, it was only known that the prediction model was correct in the case of Kalman filter with simulated data. To validate the modeling, similar tests with different sets of data—$1\,000$ simulated and $1\,000$ authentic sets—were conducted in a batch and the performance of the three approaches were logged. A new set of data was half-integrated for every simulation run whereas the authentic data sets were obtained by taking consecutive disjoint sections of $2\,000$ samples from a long set of data. In each run, the first $1\,000$ samples were used for calibration and the rest $1\,000$ samples for prediction.

The results of the batch runs are shown in Table I. It can be seen that both of the proposed methods yield a lower

TABLE I
PERFORMANCE OF THE PREDICTION APPROACHES. ABBREVIATIONS: KF: KALMAN FILTER; MA: MOVING AVERAGE; CM: CALIBRATION DATA MEAN; IE: INTEGRATED ERROR; RSSE: ROOT SUM OF SQUARED ERRORS.

	Simulated			Real data		
	KF	MA	CM	KF	MA	CM
mean IE	-119	-142	-115	-0.0214	-0.0258	-0.0728
IE std	2120	2210	2280	3.86	3.92	4.22
mean RSSE	136	139	138	0.390	0.393	0.394
RSSE std	23.3	25.4	24.9	0.0326	0.0339	0.0350

average IE than the traditional CM approach with authentic data whereas CM shows best performance in simulations, but the error standard deviations are fairly large. Dividing the error standard deviations by $\sqrt{1000}$ gives the standard deviations of the sample means; the differences in IE are smaller than these standard deviations. Therefore, these differences cannot be regarded as significant.

In contrast, the differences in RSSE between KF and the other approaches are more considerable. Between the MA and CM methods there is a one-sigma difference in favor of CM in the simulations and vice versa with authentic data, but the KF mean RSSE is smaller by two sigmas in the simulated runs and by four sigmas with real data than the CM mean RSSE. This is in accordance with the optimality of KF among linear estimators and, on the other hand, suggests that the models used in the KF are appropriate.

VI. CONCLUSIONS

In this article, two methods for predicting the evolution of the additive bias of a MEMS gyro were presented and compared to the traditional approach of plain averaging. The results suggested that one of the proposed methods, i.e., the KF approach, yields more accurate estimates in the RSSE sense, but the integral errors, which are of more importance in gyro applications, were not as significantly smaller. Another advantage of the KF is that it directly allows for computation of confidence intervals; the results showed that the obtained bounds are consistent with the data. Knowing the variance of the bias estimate is important when the measurements are used for position computations because the uncertainty in the gyro bias estimate affects the uncertainty of the resulting position solution.

The optimality property of the Kalman filter is only valid given that the models used are correct. Therefore, it is important to ensure that the environmental conditions are not changing during the calibration and prediction phases; for instance, temperature fluctuations or sudden vibrations may affect the gyro bias. In this study, these factors were mitigated by using a temperature-conditioned sensor with vibration isolation.

As future work, the fractional integration model, possibly with different choices of d, could be compared with AR models obtained using system identification algorithms, such as in [22], in terms of both model structure and prediction performance. A performance comparison could be made for the moving average estimator as well in order to see if the extra complexity of the AR models pays off. Moreover, confidence interval estimators should be derived for these suboptimal predictors. Given the estimate variances of the different methods it would be easier to decide if for a particular application it is sufficient to use, e.g., the simpler MA method instead of the computationally demanding KF approach, despite the degraded prediction performance.

REFERENCES

[1] N. Yazdi, F. Ayazi, and K. Najafi, "Micromachined inertial sensors," *Proc. IEEE*, vol. 86, no. 8, pp. 1640–1659, Aug. 1998.

[2] N. Barbour and G. Schmidt, "Inertial sensor technology trends," *IEEE Sensors J.*, vol. 1, no. 4, pp. 332–9, Dec. 2001.

[3] V. G. Peshekhonov, "Gyroscopic navigation systems: Current status and prospects," *Gyroscopy and Navigation*, vol. 2, pp. 111–118, 2011.

[4] P. Savage, "Strapdown inertial navigation integration algorithm design," *J. Guid. Control Dynam.*, vol. 21, no. 1–2, 1998.

[5] J. Rios and E. White, "Fusion filter algorithm enhancements for a MEMS GPS/IMU," in *Proc. ION ITM*, Jan. 2002, pp. 126–137.

[6] G. Dissanayake, S. Sukkerieh, E. Nebot, and H. Durrant-Whyte, "The aiding of a low-cost strapdown inertial measurement unit using vehicle model constraints for land vehicle applications," *IEEE Trans. Robot. Autom.*, vol. 17, no. 5, pp. 731–747, Oct. 2001.

[7] iSense LLC, "AIST-350 data sheet," 2010. [Online]. Available: http://www.isense.ru/products_aist350.htm

[8] M. El-Diasty, A. El-Rabbany, and S. Pagiatakis, "Temperature variation effects on stochastic characteristics for low-cost MEMS-based inertial sensor error," *Meas. Sci. Technol.*, vol. 18, pp. 3321–3328, Nov. 2007.

[9] B. M. Renkoski, "The effect of carouseling on MEMS IMU performance for gyrocompassing applications," S.M. thesis, Massachusetts Institute of Technology, 2008.

[10] "IEEE standard for inertial sensor terminology," *IEEE Std 528-2001*, Nov. 2001.

[11] J. B. Johnson, "The Schottky effect in low frequency circuits," *Phys. Rev.*, vol. 26, pp. 71–85, Jul. 1925.

[12] K. Shimotsu and P. Phillips, "Exact local Whittle estimation of fractional integration," *Ann. Stat.*, vol. 33, no. 4, pp. 1890–1933, 2005.

[13] M. S. Keshner, "$1/f$ noise," *Proc. IEEE*, vol. 70, no. 3, pp. 212–218, Mar. 1982.

[14] J. R. M. Hosking, "Fractional differencing," *Biometrika*, vol. 68, no. 1, pp. 165–176, 1981.

[15] R. F. Voss, "$1/f$ (flicker) noise: A brief review," in *Proc. 33rd Ann. Symp. Frequency Control*, 1979, pp. 40–6.

[16] M. Park and Y. Gao, "Error and performance analysis of MEMS-based inertial sensors with a low-cost GPS receiver," *Sensors*, vol. 8, no. 4, pp. 2240–2261, Mar. 2008.

[17] A. Saxena, G. Gupta, V. Gerasimov, and S. Ourselin, "In use parameter estimation of inertial sensors by detecting multilevel quasi-static states," in *Lect. Notes Artif. Int.*, R. Khosla, R. Howlett, and L. Jain, Eds. Springer Berlin/Heidelberg, 2005, vol. 3684, pp. 595–601.

[18] D. Jurman, M. Jankovec, R. Kamnik, and M. Topič, "Calibration and data fusion solution for the miniature attitude and heading reference system," *Sensors Actuat. A*, vol. 138, no. 2, pp. 411–420, 2007.

[19] W. T. Fong, S. K. Ong, and A. Y. C. Nee, "Methods for in-field user calibration of an inertial measurement unit without external equipment," *Meas. Sci. Technol.*, vol. 19, no. 8, Aug. 2008.

[20] S. Nassar, K. P. Schwarz, N. El-Sheimy, and A. Noureldin, "Modeling inertial sensor errors using autoregressive (AR) models," *Navigation*, vol. 51, no. 4, pp. 259–268, 2004.

[21] D. M. W. Abeywardena and S. R. Munasinghe, "Recursive least square based estimation of MEMS inertial sensor stochastic models," in *5th Int. Conf. Inform. Autom. Sustainability*, Dec. 2010, pp. 424–428.

[22] J. Georgy, A. Noureldin, M. J. Korenberg, and M. M. Bayoumi, "Modeling the stochastic drift of a MEMS-based gyroscope in gyro/odometer/GPS integrated navigation," *IEEE Trans. Intell. Transp. Syst.*, vol. 11, no. 4, pp. 856 –872, Dec. 2010.

[23] D. H. Titterton and J. L. Weston, *Strapdown inertial navigation technology*, 2nd ed. Peter Peregrinus Ltd, 2004.

[24] N. I. Krobka, "Differential methods of identifying gyro noise structure," *Gyroscopy and Navigation*, vol. 2, pp. 126–137, 2011.

[25] "IEEE standard specification format guide and test procedure for single-axis laser gyros," *IEEE Std 647-1995*, 1996.

[26] D. W. Allan, "Statistics of atomic frequency standards," *Proc. IEEE*, vol. 54, no. 2, pp. 221–30, 1966.

[27] R. P. Leland, "Mechanical-thermal noise in MEMS gyroscopes," *IEEE Sensors J.*, vol. 5, no. 3, pp. 493–500, Jun. 2005.
[28] W. Schottky, "Über spontane Stromschwankungen in verschiedenen Elektrizitätsleitern," *Ann. Phys.*, vol. 362, no. 23, pp. 541–567, 1918.
[29] J. Beran, *Statistics for Long-Memory Processes*. Chapman & Hall/CRC, 1994.
[30] D. Sierociuk and A. Dzielinski, "Fractional Kalman filter algorithm for the states, parameters and order of fractional system estimation," *Int. J. Appl. Math. Comput. Sci.*, vol. 16, no. 1, pp. 129–40, 2006.
[31] R. E. Kalman, "A new approach to linear filtering and prediction problems," *Trans. ASME–J. Basic Eng.*, vol. 82, no. 1, pp. 35–45, 1960.
[32] D. Sierociuk, I. Tejado, and B. M. Vinagre, "Improved fractional Kalman filter and its application to estimation over lossy networks," *Signal Process.*, vol. 91, no. 3, pp. 542–552, Mar. 2011.
[33] J. K. Roberge, *Operational amplifiers: theory and practice*. John Wiley & Sons, 1975.
[34] C. Huang, Z. Liao, and L. Zhao, "Synergism of INS and PDR in self-contained pedestrian tracking with a miniature sensor module," *IEEE Sensors J.*, vol. 10, no. 8, pp. 1349–1359, Aug. 2010.
[35] Analog Devices Inc., "ADXRS150 data sheet," 2004. [Online]. Available: http://www.analog.com/static/imported-files/data_sheets/ADXRS150.pdf

PLACE PHOTO HERE

Martti Kirkko-Jaakkola received his M.Sc. (Hons.) degree from Tampere University of Technology, Finland, in 2008, majoring in mathematics.

Currently, he is a graduate student and works as a Researcher at the Department of Computer Systems, Tampere University of Technology, where his research interests include precise satellite positioning, low-cost MEMS sensors, and indoor positioning.

PLACE PHOTO HERE

Jussi Collin received his M.Sc. and Dr.Tech. degrees from Tampere University of Technology, Finland, in 2001 and 2006, respectively, specializing in sensor-aided personal navigation.

He is currently a Research Fellow at the Department of Computer Systems, Tampere University of Technology. His research is focused on statistical signal processing of MEMS motion sensors and novel MEMS-based navigation applications. He is named inventor on several patents in the field of navigation.

PLACE PHOTO HERE

Jarmo Takala received his M.Sc. (Hons.) degree in electrical engineering and Dr.Tech. degree in information technology from Tampere University of Technology, Tampere, Finland (TUT) in 1987 and 1999, respectively.

From 1992 to 1995, he worked a Research Scientist at VTT-Automation, Tampere, Finland. Between 1995 and 1996, he was a Senior Research Engineer at Nokia Research Center, Tampere, Finland. From 1996 to 1999, he was a Researcher at TUT. Currently, he is Professor in Computer Engineering at TUT and Head of the Department of Computer Systems of TUT. His research interests include circuit techniques, parallel architectures, and design methodologies for digital signal processing systems.

Prof. Takala was Associate Editor for IEEE Transactions on Signal Processing during 2007–2011, and in 2012–2013 he is Chair of IEEE Signal Processing Society's Design and Implementation of Signal Processing Systems Technical Committee.